SCIENCE CHINA
Earth Sciences

•RESEARCH PAPER•

January 2021 Vol.64 No.1: 10–26
https://doi.org/10.1007/s11430-020-9656-8

Understanding the dynamical-microphysical-electrical processes associated with severe thunderstorms over the Beijing metropolitan region

Xiushu QIE[1,8*], Shanfeng YUAN[1], Zhixiong CHEN[1,8], Dongfang WANG[1], Dongxia LIU[1], Mengyu SUN[1,8], Zhuling SUN[1], Abhay SRIVASTAVA[1], Hongbo ZHANG[1], Jingyu LU[1,8], Hui XIAO[2,8], Yongheng BI[1], Liang FENG[2], Ye TIAN[3,9], Yan XU[4,10], Rubin JIANG[1], Mingyuan LIU[1,8], Xian XIAO[3], Shu DUAN[1], Debin SU[4], Chengyun SUN[3], Wenjing XU[1], Yijun ZHANG[5,11], Gaopeng LU[1], Da-Lin ZHANG[5,12], Yan YIN[6] & Ye YU[7]

[1] *Key Laboratory of Middle Atmosphere and Global Environment Observation (LAGEO), Institute of Atmospheric Physics, Chinese Academy of Sciences, Beijing 100029, China;*
[2] *Key Laboratory of Cloud-Precipitation Physics and Severe Storms (LACS), Institute of Atmospheric Physics, Chinese Academy of Sciences, Beijing 100029, China;*
[3] *Institute of Urban Meteorology, China Meteorological Administration, Beijing 100089, China;*
[4] *College of Atmospheric Science, Chengdu University of Information Technology, Chengdu 610225, China;*
[5] *State Key Laboratory of Severe Weather, Chinese Academy of Meteorological Sciences, Beijing 100081, China;*
[6] *Key Laboratory for Aerosol-Cloud-Precipitation of China Meteorological Administration, Nanjing University of Information Science & Technology, Nanjing 210044, China;*
[7] *Key Laboratory of Land Surface Process and Climate Change in Cold and Arid Regions, Northwest Institute of Eco-Environment and Resources, Chinese Academy of Sciences, Lanzhou 730000, China;*
[8] *College of Earth and Planetary Science, University of Chinese Academy of Science, Beijing 100049, China;*
[9] *Meteorological Observation Centre, Beijing Meteorological Bureau, Beijing 100081, China;*
[10] *Jiangxi Weather Modification, Nanchang 330096, China;*
[11] *Department of Atmospheric and Oceanic Sciences & Institute of Atmospheric Sciences, Fudan University, Shanghai 200438, China;*
[12] *Department of Atmospheric and Oceanic Science, University of Maryland, Maryland 20742, USA*

Received March 11, 2020; revised June 28, 2020; accepted July 7, 2020; published online October 19, 2020

Abstract The Dynamical-microphysical-electrical Processes in Severe Thunderstorms and Lightning Hazards (STORM973) project conducted coordinated comprehensive field observations of thunderstorms in the Beijing metropolitan region (BMR) during the warm season from 2014 to 2018. The aim of the project was to understand how dynamical, microphysical and electrical processes interact in severe thunderstorms in the BMR, and how to assimilate lightning data in numerical weather prediction models to improve severe thunderstorm forecasts. The platforms used in the field campaign included the Beijing Lightning Network (BLNET, consisting of 16 stations), 2 X-band dual linear polarimetric Doppler radars, and 4 laser raindrop spectrometers. The collaboration also made use of the China Meteorological Administration's mesoscale meteorological observation network in the Beijing-Tianjin-Hebei region. Although diverse thunderstorm types were documented, it was found that squall lines and multicell storms were the two major categories of severe thunderstorms with frequent lightning activity and extreme rainfall or unexpected local short-duration heavy rainfall resulting in inundations in the central urban area, influenced by the terrain and environmental conditions. The flash density maximums were found in eastern Changping District, central and eastern Shunyi District, and the central urban area of Beijing, suggesting that the urban heat island effect has a crucial role in the

* Corresponding author (email: qiex@mail.iap.ac.cn)

intensification of thunderstorms over Beijing. In addition, the flash rate associated with super thunderstorms can reach hundreds of flashes per minute in the central city regions. The super (5% of the total), strong (35%), and weak (60%) thunderstorms contributed about 37%, 56%, and 7% to the total flashes in the BMR, respectively. Owing to the close connection between lightning activity and the thermodynamic and microphysical characteristics of the thunderstorms, the lightning flash rate can be used as an indicator of severe weather events, such as hail and short-duration heavy rainfall. Lightning data can also be assimilated into numerical weather prediction models to help improve the forecasting of severe convection and precipitation at the cloud-resolved scale, through adjusting or correcting the thermodynamic and microphysical parameters of the model.

Keywords Lightning 3D location, Dual linear polarimetric Doppler radar, Severe thunderstorm, Lightning data assimilation, Hail, Short-term heavy precipitation

Citation: Qie X, Yuan S, Chen Z, Wang D, Liu D, Sun M, Sun Z, Srivastava A, Zhang H, Lu J, Xiao H, Bi Y, Feng L, Tian Y, Xu Y, Jiang R, Liu M, Xiao X, Duan S, Su D, Sun C, Xu W, Zhang Y, Lu G, Zhang D L, Yin Y, Yu Y. 2021. Understanding the dynamical-microphysical-electrical processes associated with severe thunderstorms over the Beijing metropolitan region. Science China Earth Sciences, 64(1): 10–26, https://doi.org/10.1007/s11430-020-9656-8

1. Introduction

Lightning disaster weather systems, also known as severe thunderstorms, are a type of strong convective weather system that usually produces heavy rainfall, lightning, hail, strong winds, tornadoes, and flood disasters (e.g., Zhang et al., 2011; Wu et al., 2013; Xia et al., 2015; Guo et al., 2017; Yang and Sun, 2018; Li et al., 2018; Ribaud et al., 2016). Lightning is one of the most typical catastrophic weather events of thunderstorm systems. In China, there are dozens of lightning strike accidents causing economic losses of over one million Yuan every year, and the number of casualties due to lightning is more than 1000 per year (Ma et al., 2008). For example, on 12 August 1989, 19 people were killed, and 78 people were injured by a lightning strike at the Huangdao Oil Depot in Shandong Province. The direct economic loss at that time was 40 million Yuan, and the indirect economic loss was nearly 100 million Yuan. On 26 June 2004, in Duqian village, Zhejiang Province, a lightning flash struck a tree, killing 17 people and injuring 13 people who had sheltered under the tree from the rain. Understanding and forecasting the development of severe thunderstorms to mitigate their detrimental impacts remains challenging (Mu et al., 2017; Luo et al., 2017; Meng et al., 2019; Qie and Zhang, 2019).

The Beijing metropolitan region (BMR) is one of the most developed areas in China, and it is also a region where significantly influenced by severe thunderstorms.The BMR frequently experiences severe thunderstorms and heavy rainfall during the summer season when the southwesterly monsoonal flow interacts with the local complex topography (e.g., Miao et al., 2011; Xiao et al., 2017; Liu et al., 2020). Lightning weather often causes large-scale flight delays and cancellations at Beijing Capital International Airport, with serious social impacts. Severe thunderstorms are one of the primary concerns of not only weather forecasters but also the local government and the public. There is mountainous terrain in the northwest of BMR, with plains in the east and south, and Bohai Bay in the southeast. Therefore, the severe thunderstorm forecasting in this region is extremely difficult because of its complicated interactions with the topography and urban areas as well as its multiscale dynamical and thermodynamical processes. The initiation and intensification of severe thunderstorms in this region remain puzzling scientific issues that have attracted considerable research attention in the past few decades. (e.g., Wilson et al., 2010; Yang et al., 2014; Sun et al., 2015; Yu et al., 2017; Liang et al., 2018; Zhang, 2020; Sun et al., 2020a).

A nationally coordinated research effort has been conducted, for the first time, to investigate the interactions between the dynamical, microphysical, and electrical processes taking place in severe thunderstorms, which was founded as a National Key Basic Research Program (STORM973, 2014–2018) by the Ministry of Science and Technology of China. The specific scientific objectives of the program include: establishing an observational database of severe thunderstorms in the BMR; revealing the dynamical, microphysical, and electrical processes in severe thunderstorms and their interactions; exploring the physical processes and mechanisms associated with lightning initiation and propagation and connection to ground objects; and developing the methodologies of assimilating lightning data and forecasting severe thunderstorms and lightning activity. To achieve these objectives, the STORM973 project designed the following six research subjects. (1) The development and integration of observational platforms and coordinated observations of severe thunderstorms. (2) The dynamical processes and structural evolution as well as their influence on the electrical processes in severe thunderstorms. (3) The effects of microphysical processes on charge structure and lightning in thunderstorms. (4) The charge distribution and its impact on lightning initiation and development in thunderclouds. (5) The charge transport by lightning and the process of attachment to ground objects. (6) The development of assimilating lightning data and forecasting severe thunderstorms and lightning.

While the STORM973 project conducted coordinated ob-

servations of thunderstorms in the BMR, as part of the STORM973 project, rocket-triggered lightning experiments were carried out in Zhanhua, Shandong Province (Sun et al., 2014; Lu et al., 2016, 2018; Jiang et al., 2017; Qie et al., 2017; Pu et al., 2017, 2019; Fan et al., 2018, 2019), and Conghua, Guangdong Province (Chen et al., 2016, 2018a, 2018b; Zhang C et al., 2017; Zhang et al., 2018) to study lightning physics and effects and attachment processes by taking advantage of the existing platforms at both bases, together with observations of high-structure-initiated lightning in Guangzhou (Gao et al., 2014; Lu et al., 2015, 2016; Qi et al., 2016; Zhang Y et al., 2017) and in Beijing (Jiang et al., 2014; Yuan et al., 2017; Wang Z et al., 2016). Observations of the electrification and charge structure of plateau thunderstorms were conducted in Datong, Qinghai Province (Wu et al., 2016; Li Y et al., 2017). Owing to length constraints, this article focuses primarily, though not exclusively, on the STORM973 campaign field in the BMR to demonstrate how it was designed and what kind of data associated with a diversity of thunderstorms were archived to help understand the different processes taking place in these storms. Some preliminary achievements are also highlighted.

2. Coordinated observation of severe thunderstorms and primary equipment

The STORM973 program brought together complementary thunderstorm observation platforms in the BMR. The field campaigns were conducted during the warm season (June–September) from 2014 to 2018. The purposes of the campaign were to comprehensively understand the various kinds of high-impact thunderclouds that might be damaging or cause flooding, and, in particular, to identify the lightning characteristics in different types of thunderstorm, and to explore the relationships between lightning and dynamical and microphysical characteristics in severe thunderstorms.

The basic geographical layout of the platforms for the campaign is shown in Figure 1, showing the distribution of the 16-station lightning detection network, i.e., the Beijing Lightning Network (BLNET), 2 research X-band polarimetric Doppler radars, and 4 raindrop spectrometers. The two radars were installed in the IAP (Institute of Atmospheric Physics) and Shunyi (SY) approximately 35 km apart, hereafter LAGEO-IAP radar and LACS-SY radar. The campaign also integrated 5 operational S-band and C-band Doppler radars, cloud-to-ground (CG) lightning location systems, rain gauges, radio sounding, automatic weather stations, and so on in the region.

The BLNET is a three-dimensional (3D) lightning location network covering most of the BMR. The waveform of lightning pulses is analyzed to distinguish CG events from intracloud (IC) flashes at each station and then the type of pulse and the arrival time of each pulse are transmitted to the IAP data center for 3D real-time location or post 3D lightning mapping with high temporal resolution (Yuan et al., 2020). A fast/slow antenna, a magnetic antenna, and a very high frequency (VHF) antenna are integrated at each station alternately to detect electromagnetic signals radiated from lightning at different frequency bands. Four different kinds of sensors cover a bandwidth from very low frequency (VLF) to VHF. The Chan and Ho (1994) algorithm and the common Levenberg–Marquardt (LM) algorithm are jointly utilized in the BLNET location techniques (Wang Y et al., 2016). All stations have been upgraded to provide better detection of lightning signals in the megacity cluster area under complex background radiofrequency noises. The average detection efficiency for total flashes is 93.2%, and the identification efficiency for CG flashes is 73.9% (Srivastava et al., 2017). To reduce the interference of the complex electromagnetic environment with the lightning signals, the equipment at all sites is continuously upgraded and improved. Two high-speed cameras are installed at the IAP station to capture tall-structure lightning for lightning physics studies and BLNET performance evaluation. The horizontal location error of the BLNET for tower-initiated lightning flashes ranges from 50 to 250 m.

Polarimetric radar has the capability to remotely identify a variety of hydrometeor types, such as graupel, snow, large and small hail, and mixed-phase precipitation. However, X-band radar suffers from large attenuation during heavy rainfall and needs to be corrected before it can be used for hydrometeor identification (Feng et al., 2018). Furthermore, like all other remote-sensing approaches, *in situ* verification is needed for this polarimetric-based hydrometeor classification. Four raindrop spectrometers were installed in the common observation area of the two X-band radars for this reason. The processing and analysis of X-band radar data will not be discussed here.

A total of 220 thunderstorm cases were observed during the five summers of the field campaign. The documented thunderstorms spanned different organizational categories, from small-sized single convective cells to various types of multicell convective systems (MCSs), as well as squall lines and occasionally supercells. Table 1 lists some of the major thunderstorms during the STORM973 campaign. Although a diverse range of thunderstorms was observed, they can be divided into three major categories: single-cell thunderstorms, multi-cell thunderstorms, and squall line storms. Years of observation have found that squall lines and multicell thunderstorms are the two major categories of severe thunderstorms in the BMR. A squall line is a type of MCS with a convection line at the front and a trailing stratiform region, and it usually produces extreme rainfall in the central urban area, occasionally causing flash flood disasters, whereas a multicell storm usually produces local

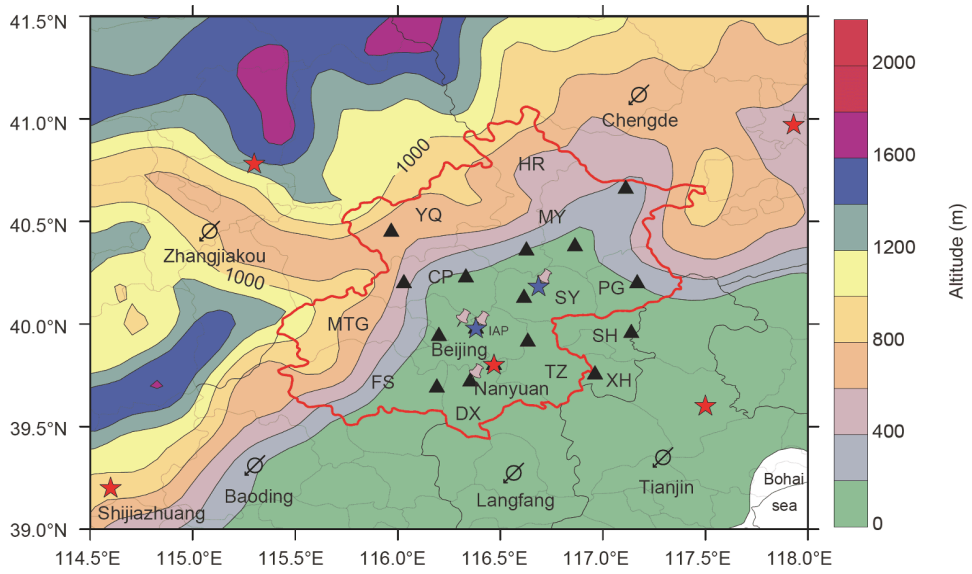

Figure 1 The layout of the comprehensive observational platform for severe thunderstorms in Beijing. The 16 black triangles represent the BLNET stations. The stars represent the radar stations, with blue for X-band (LAGEO-IAP radar and LACS-SY radar) and red for the 5 operational S-band or C-band Doppler radar. The pink pins are the 4 raindrop spectrometers. The red polygon shows the boundary of Beijing city, and the color shading delineates the terrain height above sea level with at intervals of 200 m.

Table 1 Major thunderstorm categories during STORM973 campaign

Storm category	Observation period each year					
	2014-05-10–09-30	2015-06-06–09-11	2016-05-11–09-25	2017-06-13–09-24	2018-05-15–08-25	Total
Single cell (4 supercells)	20	15	13	13	14	75
Multicell	15	29	26	24	27	121
Squall line	4	7	8	4	1	24
Total	39	51	47	41	42	220

short-duration heavy rainfall. It is still challenging to predict these two types of thunderstorm, especially for frequent clustered meso-γ-scale cells. Supercell is another type of severe thunderstorm, but does not frequently occur in the BMR, just four times during the five-year observation campaign.

Table 2 lists some severe thunderstorm cases and the associated weather phenomenon. The peak flash rates and percentages of positive CG flashes that occurred within the coverage of the BLNET are also listed. It should be pointed out that, in this study, several radiation sources detected by the BLNET are grouped together as a single lightning flash. When the time interval of the located radiation pulses is less than 400 ms, with a horizontal distance of less than 15 km, they are grouped into the same lightning flash, and the total duration of a flash is limited as less than 1.5 s. For a grouped lightning flash, at least two radiation pulses are required, that is, flashes with only one radiation pulse are excluded and classified as noise data. After this grouping process, a single lightning flash usually contains several to thousands of radiation points, which is determined by various factors such as duration of the flash, intensity of the radiation, background radio interference, and number of stations that receive the lightning signal.

It can be seen that the squall line MCSs show a very high total flash rate (maximum >1 flashes s^{-1}) and are usually accompanied by hails. The maximum total flash rate of the four supercell storms varies from 0.3 to 6.8 flashes s^{-1}, with hail occurring in all cases, and the corresponding +CG flash ratio is also high, ranging from 24% to 50%. The multicell thunderstorms usually consist of several rapidly developing meso-γ-scale convective cells and cause local hail and lightning, and sometimes local flash floods in the city without obvious precursors. As multiple meso-γ-scale convective cells may occur at different locations at the same time or in succession, the overall spatial scope and timescale may be large, heavily affecting the normal operation of various national infrastructures and public utilities. In the following section, a typical case of each of these three types of severe thunderstorms is discussed in detail.

Table 2 Some severe thunderstorm cases, along with the description of the severity report associated with the storms and the detection data[a)]

Date	Storm type	Severity description	Max. flash rate (flashes s^{-1})	Max. half-hourly +CG Ratio (%)	Available observations
13 Jun 2014	Supercell	Hail, wind gust, heavy rainfall	2.7	50	1, 2, 3, 4, 5, 6, 7
26 Jun 2015	Cell	wind gust, heavy rainfall	0.7	54	1, 2, 3, 4, 5, 6, 7
27 Jul 2015	Squall line	Hail, wind gust, heavy rainfall	6.2	30	1, 2, 3, 4, 5, 6, 7
5 Aug 2015	Multicell	Wind gust, heavy rainfall	0.6	50	1, 2, 3, 4, 5, 6, 7
7 Aug 2015	Squall line	Hail, wind gust, heavy rainfall	4.1	33	1, 2, 3, 4, 5, 6, 7
10 Jun 2016	Multicell	Hail, wind gust	3.2	53	1, 5, 6, 7
23 Jun 2016	Supercell	Hail, wind gust, heavy rainfall	0.3	24	1, 2, 3, 4, 5, 6, 7
7 Jul 2017	Squall Line	Hail, wind gust, heavy rainfall	1.1	36	1, 2, 3, 4, 5, 6, 7
13 Jul 2017	Squall Line	Wind gust, heavy rainfall	1.6	44	1, 2, 3, 4, 5, 6, 7
5 Aug 2017	Supercell	Hail, wind gust, heavy rainfall	0.5	28	1, 2, 3, 4, 5, 6, 7
8 Aug 2017	Multicell	Hail, wind gust, heavy rainfall	1.0	47	1, 2, 3, 4, 5, 6, 7
11 Aug 2017	Supercell	Hail, wind gust, heavy rainfall	6.8	24	1, 2, 3, 4, 5, 6, 7
12 Jun 2018	Multicell	Hail, wind gust, heavy rainfall	0.4	65	1, 2, 3, 4, 5, 6, 7
30 Jun 2018	Multicell	Hail, wind gust, heavy rainfall	0.4	66	1, 2, 3, 4, 5, 6, 7
15 Jul 2018	Squall line	Heavy rainfall	1.6	34	1, 2, 3, 4, 5, 6, 7

a) Available observations: 1, 3D lightning location; 2, LACS-SY radar; 3, LAGEO-IAP radar; 4, raindrop spectrometers; 5, S-band Doppler radar; 6, sounding; 7, automatic weather station (AWS). Information on hails comes from manual records of Beijing Meteorological Station.

3. Lightning activities in different thunderstorms

To understand the development characteristics of the different types of severe thunderstorms and describe the data obtained, a typical case of squall line, multicell, and supercell thunderstorms were selected for a brief review. All of these storms featured with high total (CG and IC) lightning flash rates and some of them had very high flash rates (>3 flashes s^{-1}) and high +CG flash ratios for some period during their lifetimes. The time used here is the Beijing Standard Time (BST).

3.1 The squall line on 27 July 2015

Leading-line and trailing stratiform MCSs or squall lines are regarded as one of the most intriguing types of severe thunderstorms in the BMR, some of which have been extensively studied (Xu et al., 2018; Sun et al., 2019). Here only the squall line on 27 July 2015 (referred to as the 20150727 squall line) was selected for analysis. This squall line was the most severe thunderstorm during the five-summer observation period. It initiated in the BMR under the influence of the northeast cold vortex interacting with a southwesterly warm and humid airflow associated with the subtropical high to the northwest (not shown). The Beijing radiosonde at 14:00 showed a surface water vapor mixing ratio exceeding 20 g kg^{-1}, with a substantial inversion layer at a lower altitude. The convective available potential energy (CAPE) reached 3438 J kg^{-1}, and the convection suppression energy (CIN) was very low, 20 J kg^{-1}, indicating that the prestorm environment was highly favorable for the initiation of deep convection. The squall line occurred in the evening and lasted more than 6 h. The convection system moved from the northwest to the southeast, and produced heavy precipitation in most parts of the BMR. The local cumulative precipitation exceeded 100 mm, accompanied by hail and short-term strong winds, as well as frequent lightning activity. Over 1000 flights were delayed or canceled at Beijing Capital International Airport because of the lightning.

Isolated convective cells began to appear around 18:00 in northwest and northeast Beijing based on the composite reflectivity of this case from an S-band radar, located in observatory in the southern suburbs of Beijing. Figure 2 shows the composite radar reflectivity and overlay of lightning radiation sources at several moments. It can be seen that at 18:30 (Figure 2a), a "bow-echo" convective storm formed in the west of Beijing, and there were strong convective echoes in the northeast. Both storms took place in the southwesterly flow along a cold front associated with the cold vortex, and there was weak convection activity between the two. One hour later, the two convective cells merged as they moved southeastward (Figure 2b), and they developed into a squall line morphology at 20:00 (Figure 2c). The convection line started to break at 20:30 (Figure 2d), and then gradually weakened. The analysis found that about 93% of lightning radiation sources were distributed in the convection line and the transition area about 10 km from the edge of the convection line (Xu et al., 2018). From a height perspective, the radiation sources were distributed predominately in an alti-

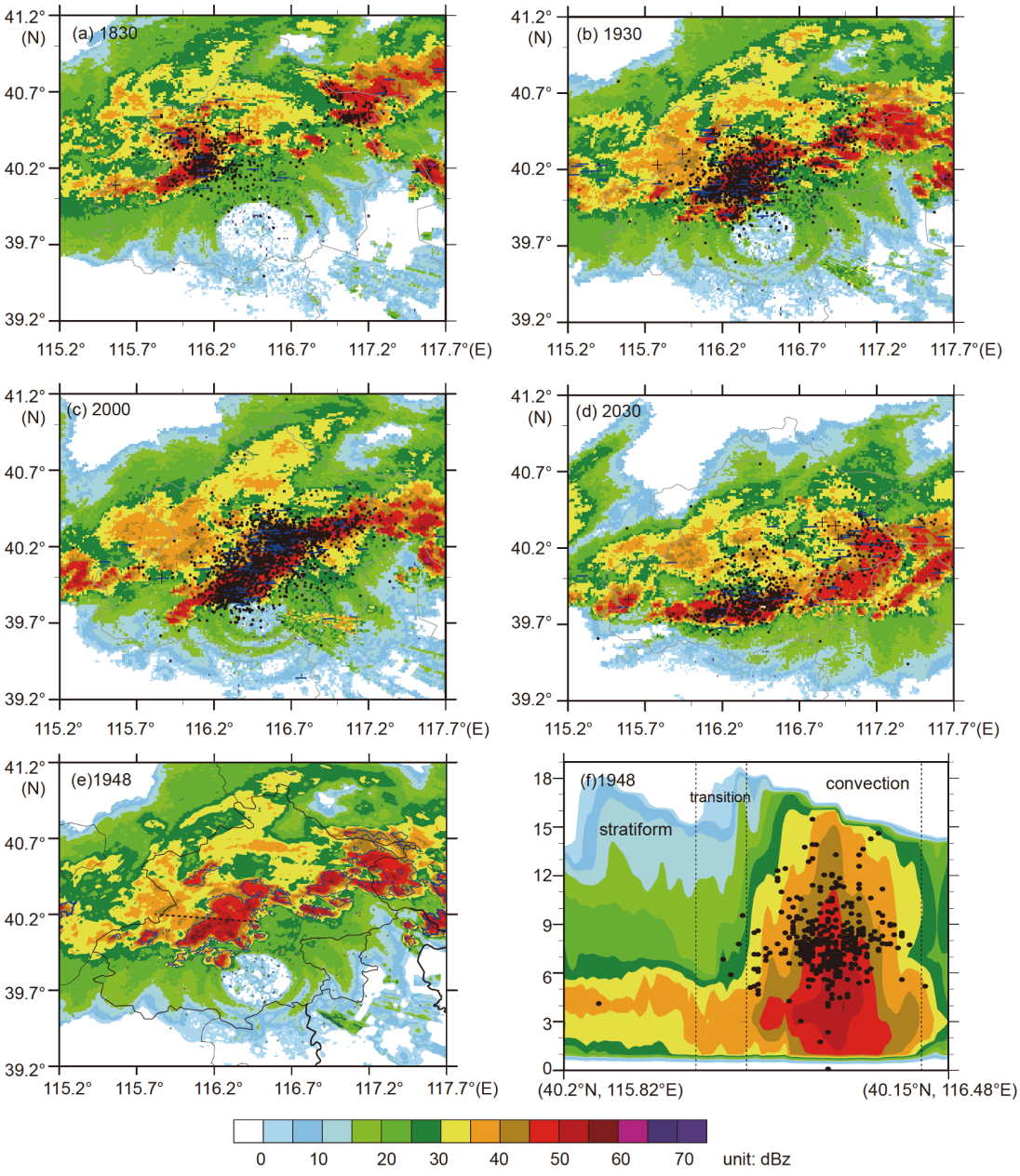

Figure 2 Composite reflectivity from the S-band radar overlapped with lightning radiation sources ("·" for IC, "–" for −CG, and "+" for +CG flash) in 6 min for the 20150727 squall line at (a) 18:30, (b) 19:30, (c) 20:00, and (d) 20:30. (e) Radar reflectivity at 19:48. The convective region is shown by the blue contour. (f) Vertical cross-section of radar reflectivity along the dotted line shown in (e) and lightning radiation sources within 0.1° (longitude or latitude) of the cross line in 6 min (same as below).

tude layer between 6 and 9 km (Figure 2f) and were mainly distributed in the convection region. A small number of radiation sources propagated along the convection line to the rear stratiform region. There were obvious bright bands in the stratiform region, but only isolated radiation sources in the bright band.

Figure 3 shows the evolution of flash rate during the thunderstorm lifetime, which is characterized by a high flash rate. IC flashes dominated during the lifetime of the thunderstorm, and the flash rate peaked at 20:18 with a value of over 2200 flashes $(6\ \text{min})^{-1}$. The CG flash rate peaked at about 20:48 with a value of 240 flashes $(6\ \text{min})^{-1}$ (Figure 3a). Positive CG flashes were active in the dissipating stage of the system. From 21:00 to 23:00, the +CG flashes account for 14% to 30% of all CG lightning flashes (Figure 3b). Xu et al. (2018) analyzed this thunderstorm process in detail and found that there was a high water vapor concentration during the convection merging process from 19:24 to 20:18, and the peak of lightning lagged 24 min behind the peak of vertically integrated liquid water content (VIL). Based on the wind field retrieved from the Variational Doppler Radar Analysis System (VDRAS) (Sun et al., 2010), the merging of the

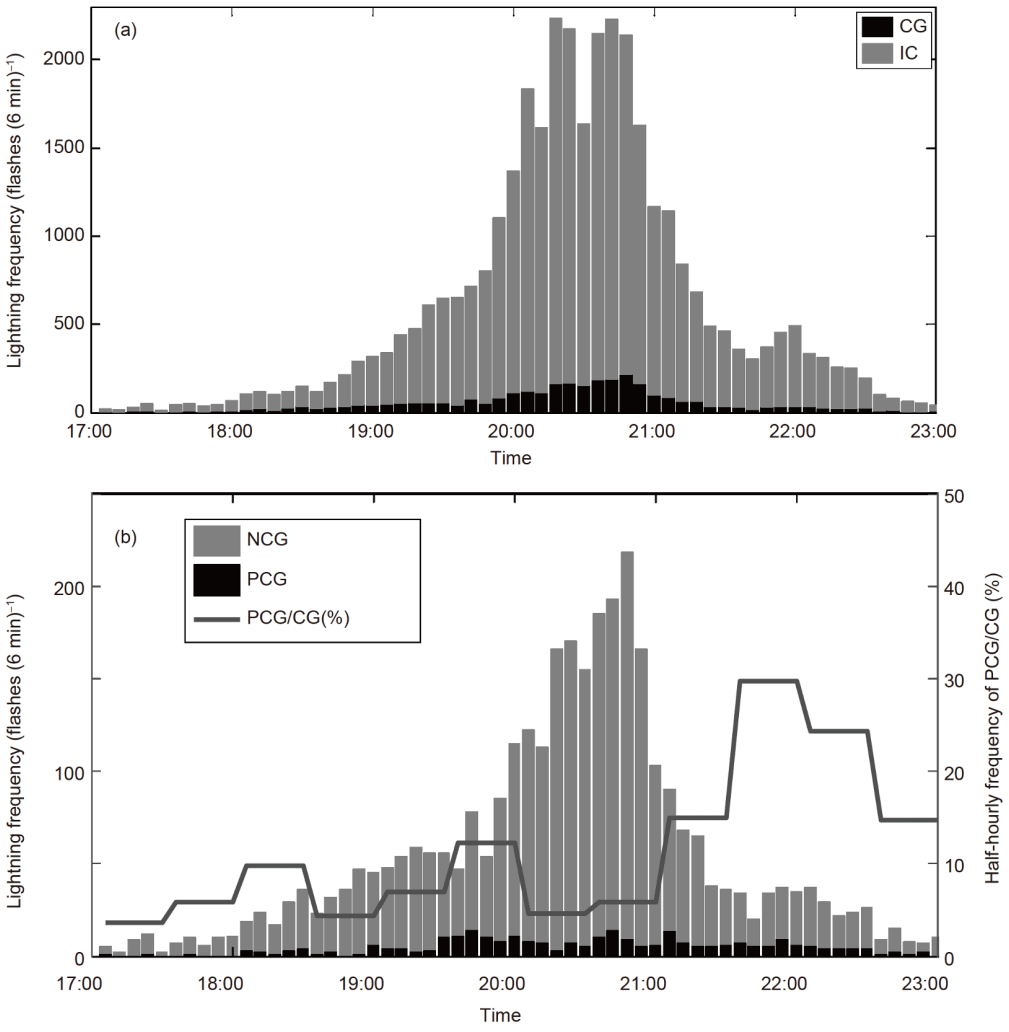

Figure 3 Evolution of lightning flash rate for the 20150727 squall line. (a) IC and CG flashes, and (b) +CG and −CG flashes, together with the half-hourly ratio of +CG to CG flashes.

convective cells mainly occurred in the lower convergence zone. After the convection merging process at 20:18, the extent and intensity of the updraft both became intense, with more active lightning activity. Lightning was mainly concentrated in the region with large vertical wind shear, while few radiation sources were located in the rear of the convection zone, consistent with the downdraft.

3.2 Multicell hailstorm on 10 June 2016

This multicell storm is an obvious hailstorm (referred to as the 20160610 multicell hailstorm). The weather map at 08:00 showed that the hailstorm process was affected by the northeast cold vortex and the high-altitude trough. The low-level warm and humid airflow in front of the 850 hPa high-altitude trough formed an obvious wet tongue, which intersected with the dry and cold northwest airflow in Beijing, forming an unstable layer (not shown). The sounding at 14:00 in Beijing showed that the CAPE value was 2726 J kg^{-1}, and there was an inversion layer near 900 hPa. The depression of the dew point below 800 hPa was small and the water vapor content was high. Above 800 hPa, the depression of the dew point was large, and the water vapor content was low. The stratification of upper dry and lower wet air provided good dynamic and thermal conditions for the outbreak of this multicell hailstorm.

The 20160610 multicell hailstorm consisted of several isolated cells triggered in sequence, with a duration of more than 5 h. Figure 4 shows the overlap of radar reflectivity and lighting radiation sources at four different times. From the radar echo at 14:54 (Figure 4a), it can be seen that two clusters of convective cells were separated from each other, with the southerly one located over Haidian District and the northerly one located over Miyun District. The north cluster moved eastward, while the south cluster moved southeastward and eventually weakened in Tianjin. According to the ground observation record from the Beijing Meteorological Station, the south cluster included five successive

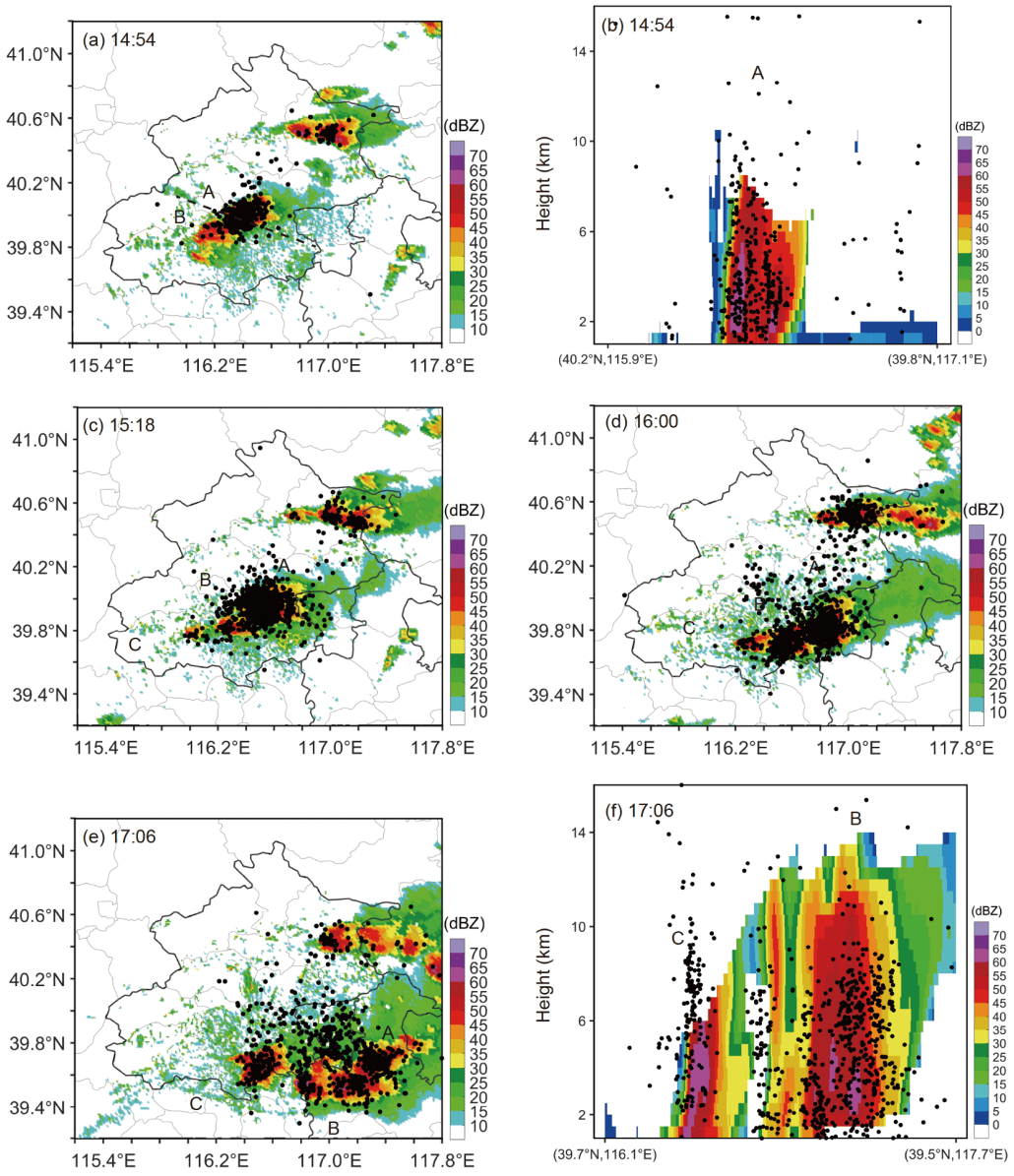

Figure 4 The radar reflectivity of the 20160610 multicell hailstorm overlapped by lightning radiation sources (black dots) in 6 min. (b) and (f) are vertical sections along the black dotted line in (a) and (e), respectively.

hailfall periods on its moving path, and here we focus on this south cluster.

Three cells successively burst out from the south cluster. Cell A first broke out at 14:20 in the northwest of Haidian District (not shown) and began to hail at 14:48, and the hailfall lasted about 12 min. During this period, a strong echo greater than 60 dBZ appeared, with a top height of about 6 km (see Figure 4b). At this time, cell B had also triggered and continuously enhanced. Cell C triggered at 15:18 (see Figure 4c), and the periphery of cell B and cell A began to merge, although the two strong convection centers were still separated. According to the human observation record from the weather station, during the developing and moving process, cell A produced hail in Haidian District (14:48–15:00, see Figure 4a and 4b), Chaoyang District (15:18–15:30, see Figure 4c), and Tongzhou District (16:00–16:06, see Figure 4d). Although the hail in the three areas was all generated by cell A, the hailfall did not last longer than 1 h, and the three hailfall periods broke out successively. The fourth hail period occurred around 16:54–17:00 and was generated by cell C when it was located near the radar station. The radar failed to detect the strong echo center, and only the weak echo area at low elevation was detected. For clarity, Figure 4e shows the radar reflectivity factor with the lightning radiation sources in 6 min at 17:06 after the end of the hail. Figure 4f shows the corresponding vertical section. It can be seen that the echo intensity was still very strong even after the hailfall. A strong echo greater than 60 dBZ still existed, and the top height

exceeded 6 km. However, the radar still failed to detect the higher cloud top. The height range obtained by the 3D location of the lightning radiation sources was mainly distributed at 2–10 km, with a maximum exceeding 14 km. As can be seen in Figure 4f, there were two 60 dBZ strong echo regions in the front and back of cell B in Tianjin, and the top height of the 40 dBZ echo exceeded 13.5 km. A few radiation sources close to the ground could be caused by individual CG flashes. The fifth hailfall from 17:24 to 17:36 occurred in Tianjin after the merging of cells A and B, and will be not discussed in detail here.

During the evolution of the hailstorms, the overall horizontal scale of the three cells was relatively small, which were all at the meso-γ-scale. However, the intensity of the convection was large, and the height of the strong echo was high. The top height of the 40 dBZ echo exceeded 13 km during most of the storm lifetime. During the hailfall stage, the strong echo of 60 dBZ appeared with a top height exceeding 11.5 km at some moments. The lighting radiation sources were mainly distributed in the strong echo area with an intensity greater than 40 dBZ, indicating that there was a strong updraft in the cloud. The updraft was conducive to the generation and growth of hail, and the ice-phase microphysical processes, in turn, strengthened the non-inducive charging mechanism in the cloud through the collision of ice particles and charge separation (Saunders and Peck, 1998), which further promoted the occurrence of lightning.

It can be seen from Figure 4 that some lightning radiation sources were distributed outside the radar echo. The main reason for this is that they came from the lightning discharge branch channel that occurred outside the cloud. The BLNET can detect most radiation pulses during the process of lightning discharge, and the radiation pulses generated by the discharge branches inside or outside the cloud can all be located. Another reason is that the weaker echo around the strong echo cannot be effectively detected by the S-band radar, and the echo area may not well reflect the true structure of the thunderstorm. Unfortunately, the two X-band radars missed the observation of this hailstorm. It should be noted that due to blockage by ground objects and the blind zone of radar at close distance, the radar detection for this hailstorm process was incomplete and most of the vertical profiles do not reflect the real thunderstorm periphery. In comparison, the 3D location of lightning radiation sources is not affected by ground objects, which can compensate for the shortage of the radar observations to some extent.

Figure 5 shows the variation of lightning flash rate and radiation source height with time for this hailstorm process. The five successive hailfall periods are marked with black lines below the abscissa of the figure. During the first hailfall

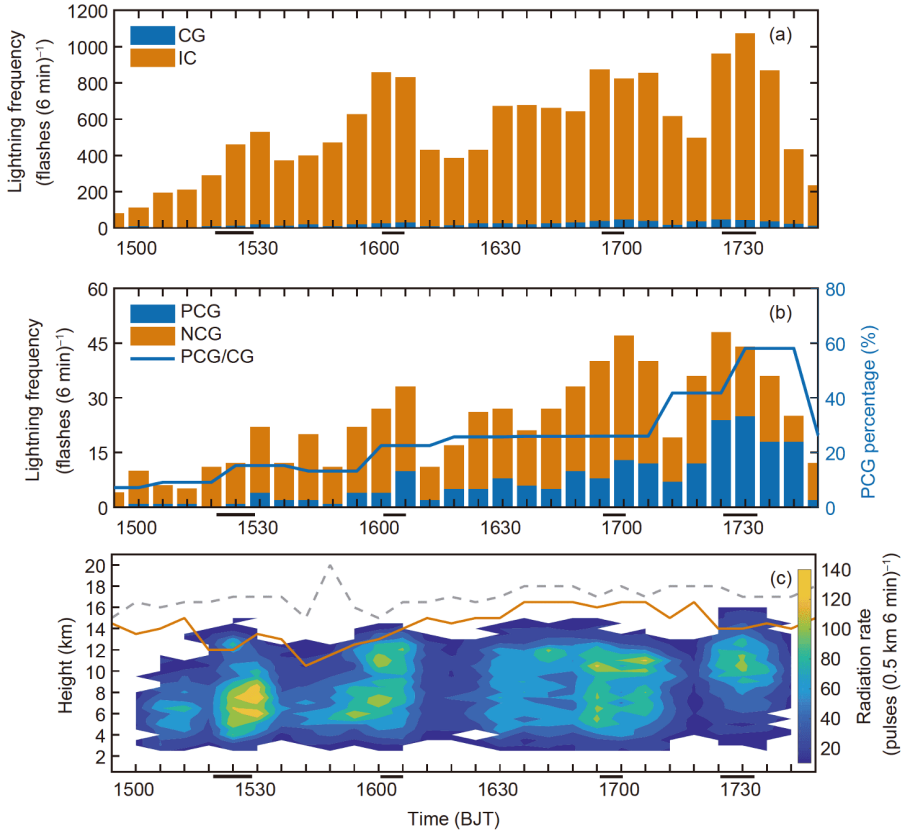

Figure 5 Variation of the flash ratio and radiation source height with time for the 20160610 multicell hailstorm. (a) CG and IC flashes and (b) −CG and +CG flashes. (c) Ratio of radiation source per 0.5 km height layer (color bar unit: pulses (0.5 km 6 min)$^{-1}$) and the variation of echo top height (unit: km) of 40 dBZ (dashed line) and 50 dBZ (solid line) with time. The black lines on the abscissa represent the hailfall stage.

stage, some of the BLNET stations had not yet started the observation, so this stage was not analyzed. Throughout the development process of the hailstorm, the IC flashes accounted for more than 80% of the total flashes, and the total flash rate reached the maximum at 15:30, 16:00, 17:00, and 17:30, corresponding to the last four hail stages. The peak flash ratio during the fifth hail stage was the highest, exceeding 1000 flashes $(6\ \text{min})^{-1}$. At this time, cell A and cell B were completely merged, and cell C after the hailfall was still in a strong stage. The multicell hailstorm was developing vigorously as a whole with a higher cloud top, so the flash ratio was high.

Figure 5c shows the evolution of the radiation source height distribution over time in this multicell hailstorm process. During the second hail stage around 15:24, the number of radiation sources of lightning discharge increased substantially, mainly concentrated between 4 and 12 km height, and the peak area appeared in the height layer around 5.5–9.0 km. In the third hailfall stage around 16:00, the radiation source distribution area expanded to a higher height level. In addition to the peak layer at about 5.5–9.0 km, the second peak of radiation source density appeared at 10–13 km. In the fourth hailfall stage at around 16:54, cells A and B began to merge, resulting in the radiation sources being active in the 4–13 km altitude layer for a longer period at four altitude layers, and hail was produced by the enhanced cell C. After a short period of no hail, the fifth hailfall stage began at 17:24, and the radiation sources were active again. The peak area of the radiation sources increased substantially around 17:30, and the height of the radiation sources was mainly distributed in the 6–13 km height layer. The peak appeared at a height of 10–12 km, with lightning radiation sources exceeding 100 pulses $(0.5\ \text{km}\ 6\ \text{min})^{-1}$ and the lightning flash ratio exceeding 1000 flashes $(6\ \text{min})^{-1}$. Compared with the previous hail stages, the total flash ratio and IC ratio of the fifth stage were the highest, and the ratio of +CG to the total CG flashes also reached the maximum, close to 60%. A high flash ratio and high +CG flash ratio are common characteristics of a hailstorm and can be used as an indicator of the occurrence of hail disasters (Feng et al., 2007; Logan, 2018; Xu S et al., 2016; Sun et al., 2020b). The ratio of +CG to the total CG flashes during the lifetime of this multicell hailstorm exceeded 20%, and the ratio increased substantially during the third, fourth, and fifth hailfall stages.

It is worth noting that the hail records used in this study came from the manual records of the Beijing Meteorological Station. Owing to the sparse stations, the start and end time of the hailfall may not be accurate, and the duration of each actual hail stage could be longer than the marks shown in Figure 5. For example, the radar reflectivity exceeded 60 dBZ for cell B and cell C at 17:06 as shown in Figure 4c, and the corresponding flash ratio was also very high (see Figure 5), which indicates hailfall. That is, the duration of the fourth hailfall stage could be longer than 12 min.

3.3 Supercell on 11 August 2017

This supercell thunderstorm process (referred to as the 20170811 supercell) caused heavy rainfall in Beijing, accompanied by hail, short-term strong winds of force 6–8, and intensive lightning activity. The average rainfall in the urban area and the eastern region was 10–30 mm, and locally exceeded 100 mm. On the basis of the weather map at 08:00 (figure not shown), there was a strong Mongolian low vortex in the mid–high latitude area at 500 hPa. The westward airflow prevailing in the south of the cold vortex was dominant over Beijing. The northerly airflow in the west of the cold vortex and the northwestern airflow behind the trough brought the dry cold air in the middle layer in the north. The low-level 850 hPa southwesterly jet was active and covered with a wet tongue. The southwesterly airflow transported a warm and humid air mass under the dry cold air mass, forming an unstable layer in the Beijing area. The sounding profile at 08:00 shows that the CAPE was as high as 3937 J kg^{-1}. The horizontal wind rotated clockwise from the lower layer to the upper layer, and there was a strong horizontal wind vertical shear, which is a favorable environmental condition to trigger strong convective weather.

In the initial stage of the 20170811 supercell, several weak cells were formed in the convergent area of southern Beijing (Figure 6a), after which the intensity and the dimensions increased rapidly. From 18:42 to 19:30, the spatial scale of strong echo increased to more than 100 km in the northeast–southwest direction (Figure 6b and 6c). At 20:00, the total flashes exceeded 1600 flashes $(6\ \text{min})^{-1}$ (Figure 7a), indicating that a large number of ice particles were generated, collided, and charged with the strong upward airflow (Saunders and Peck, 1998; Sun et al., 2018; Chen et al., 2020). After 20:00, the supercell storm entered the maturity period (Figure 6d). At this time, hail was observed on the ground (radius of hailstone >3 cm), and the total flash ratio exceeded 2000 flashes $(6\ \text{min})^{-1}$ (Figure 7a). After this, the supercell gradually weakened as it continued to develop southeastward. After 21:30, the organization of the supercell became increasingly worse (Figure 6e), and left large-scale stratiform cloud behind it. The weakened thunderstorm produced less lightning, mainly in isolated areas with high radar reflectivity (Figure 6f).

It can be seen in Figure 7 that although the decrease in the total flashes corresponds to the weakening process of the thunderstorm, the ratio of +CG flashes to total CG flashes increased substantially after 22:30, reaching a maximum of 24% (Figure 7b), with a very low lightning frequency. In the development and mature stages, the ratio of +CG lightning to total CG lightning was about 10%. The high +CG flash ratio during the thunderstorm dissipation period was a common

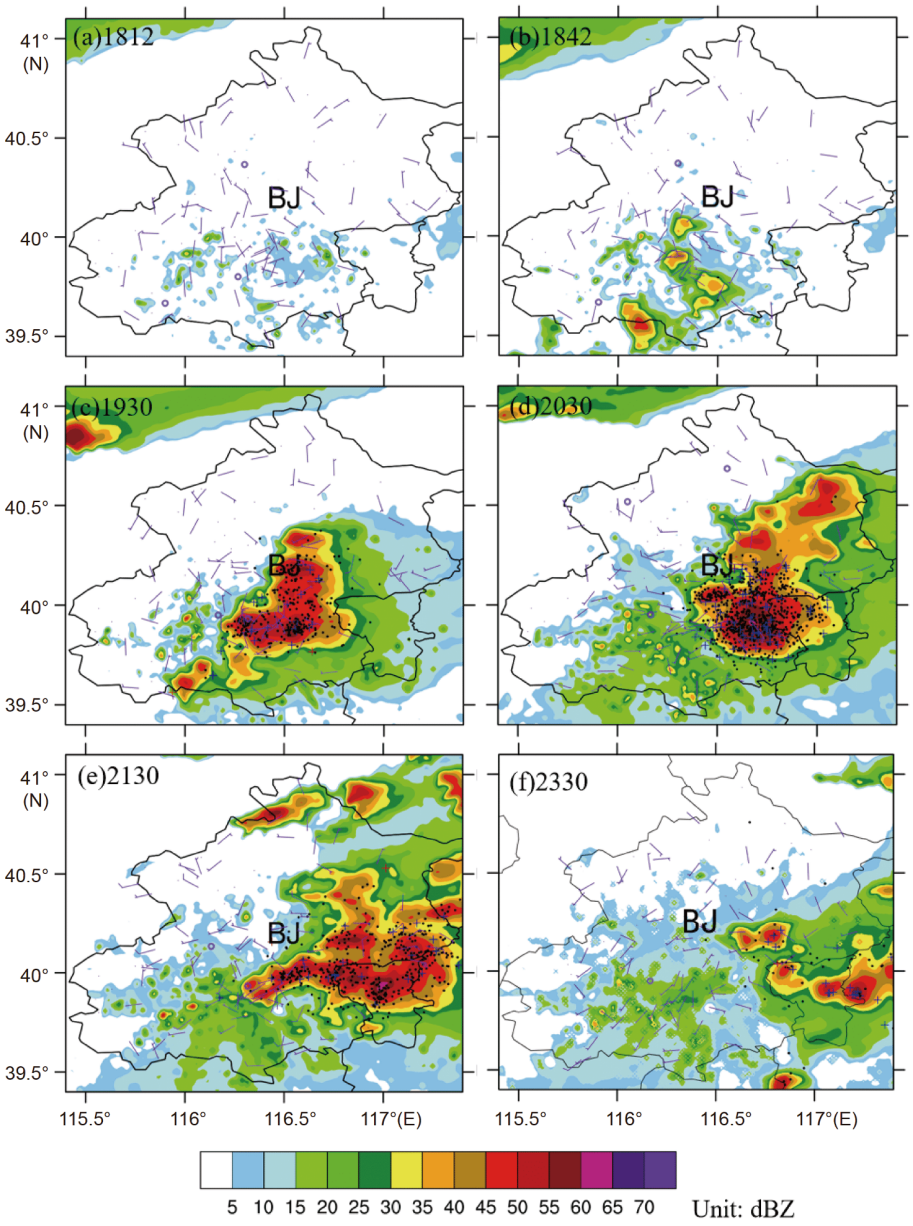

Figure 6 The composite reflectivity of the radar at six moments for the 20170811 supercell with the overlap of lightning after the group within 6 min. The wind vectors represent the surface wind field detected by the automatic weather station, and the long and short barbs represent 2 and 4 m s^{-1}, respectively.

phenomenon, mainly due to the reduction in the number of total lightning flashes and CG flashes. Of course, sometimes, owing to the thunderstorm moving far beyond the effective detection range of the lightning detection network, only some strong CG lightning can be detected, which may give the illusion of a high ratio of +CG lightning to total CG lightning. On average, +CG lightning is usually stronger with higher a peak current than −CG and IC flashes, and it can be detected at a far distance. IC flashes are relatively weak and difficult to detect when they are far away. For this process, the high +CG flash ratio was mainly due to the weakening of the supercell in the later period and the reduction of the total number of flashes. From the perspective of radar echo, the reflectivity gradually weakened after 23:00, and the lightning frequency decreased rapidly from 500 flashes $(6\ \text{min})^{-1}$. By 23:42 (Figure 6f), the radar echo splits into several scattered small cells, with a flash ratio of only 200 flashes $(6\ \text{min})^{-1}$, and the number of CG flashes and +CG flashes was only 1–3.

4. Spatial distribution of lightning and possible effects of urban heat island effect on lightning and thunderstorm intensity

It is interesting to find that all the above-mentioned cases

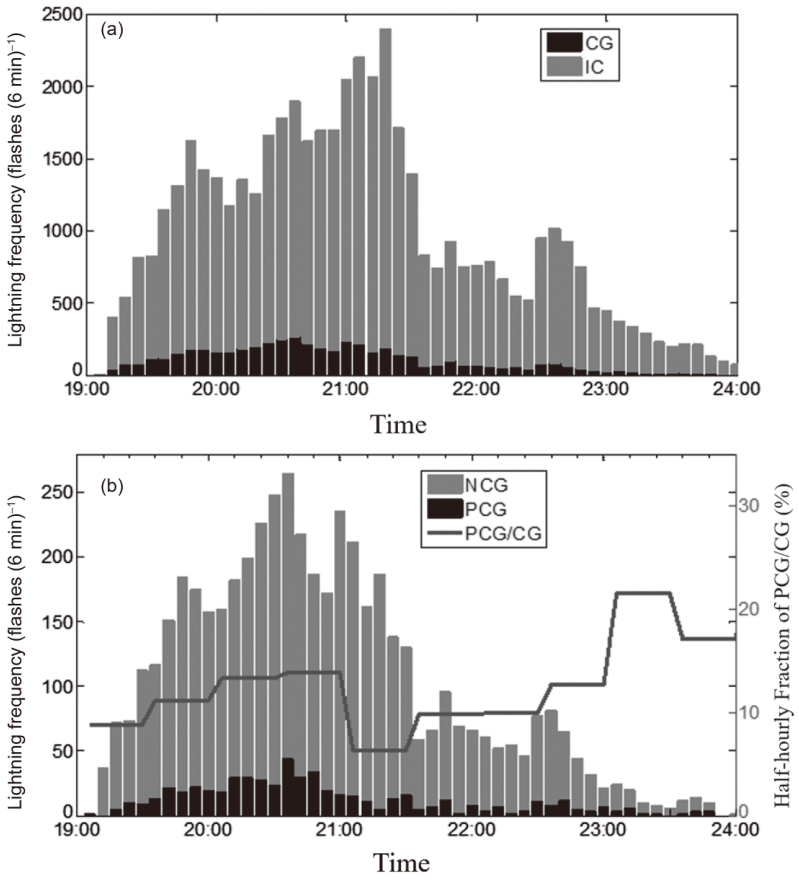

Figure 7 Evolution of the lightning flash rate with time for the 20170811 supercell. (a) IC and CG flashes, and (b) +CG and −CG flashes, together with the half-hourly ratio of +CG to CG flashes.

intensified over the urban area (southeastern plain of the BMR) even though they initiated in different mountainous locations, indicating a possible substantial urban effect on the evolution of severe thunderstorms. Figure 8 shows the spatial distribution of lightning density in the BMR. The eastern part of the Changping District, the central and eastern parts of the Shunyi District, and the main urban area of the BMR are the high-flash-density regions with a maximum density greater than 15.4 fl km^{-2} yr^{-1}. The average lightning density in the BMR is about 1.9 fl km^{-2} yr^{-1}. On the basis of the number of lightning flashes generated by a thunderstorm and the intensity and duration of the radar echo, the thunderstorms are divided into super thunderstorms (with total flash number >10000), strong thunderstorms (flash number between 1000 and 10000), and weak thunderstorms (flash number <1000). The precipitation processes that were clearly separated in space or substantially different in time were counted as different thunderstorms with reference to the radar echo. The super (5% of the total), strong (35%), and weak (60%) thunderstorms contribute about 37%, 56%, and 7% of the total flashes, respectively, and the lightning maximum centers are principally produced by strong thunderstorms and super thunderstorms (Wang et al., 2020). The super and strong thunderstorms were usually active over the urban area in evening or night after it originated in the west or northwest mountainous region and propagated eastward or southeastward, while the storm cell cluster or weak thunderstorms tend to occur in the afternoon. The high-value area in Figure 8 was close to the location of the vigorous period of the two strong MCSs, the 20150727 squall line and the 20170811 supercell. In fact, the distribution of lightning density is largely determined by the most vigorous period of strong thunderstorms and super thunderstorms.

Wind field convergence lines are affected by the terrain and environmental condition around Beijing, and are usually formed in the lower layers of atmosphere when the northwest airflow behind the high-altitude cold vortex encounters the southeast airflow from Bohai Bay. Most of the convection cells are triggered and enhanced along these convergence lines. Multiple cells can be initiated simultaneously or sequentially for a period, forming the multicell thunderstorm. However, as the cells developed and expanded, they moved closer to each other and merged, to form obvious squall line convection. Low convective inhibition and high low-level wind speed on the plain are found for both types of thunderstorms, whereas higher vertical shear over the plain and

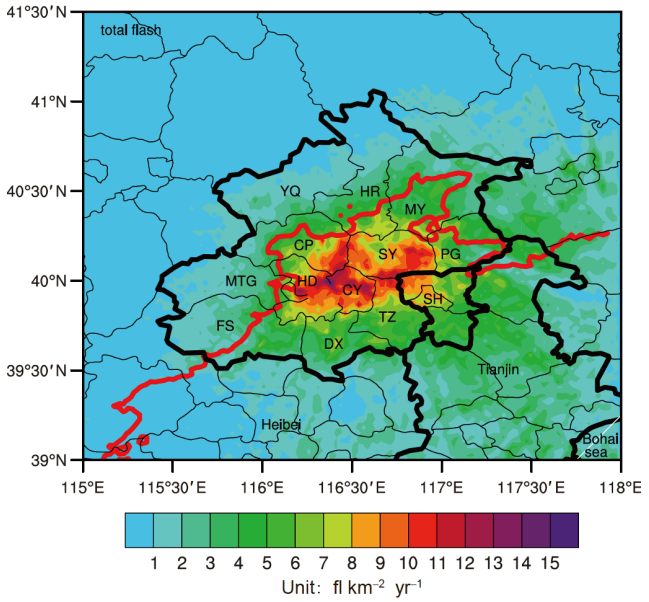

Figure 8 Annual average density distribution of total lightning flashes. The red curve shows the elevation line of 200 m above sea level.

stronger wind speed over both mountains and plains are found only for squall lines. Xiao et al. (2017, 2019) found that the stronger wind and vertical shear during the squall line process produced more intense downdrafts, resulting in a deeper cold pool, strong outflow, and convergence. These intensified the thunderstorm in the urban area and consequently produced more lightning. It is interesting to note that the lightning maximum is in the urban area, while the precipitation maximum is in the urban and downstream suburban areas. The precipitation peak is later than the lightning peak, indicating that lightning may be used for nowcasting of short-term heavy precipitation events (Wu et al., 2017, 2018; Li et al., 2017a).

The urban heat island effect plays an important role in enhancing regional precipitation (Shepherd, 2005; Zhang, 2020). Most of the Beijing thunderstorms originate in the mountainous areas in the west. As a large metropolitan city, the urban area of Beijing has a substantial impact on the local meteorological conditions. According to the STORM973 observations, the urban area has a crucial role in the intensification of thunderstorms in the BMR, especially in the central urban region. The urban heat island effect of the BMR substantially alters the heat and moisture fluxes in the urban areas compared with the neighboring rural areas (Yu et al., 2017; Lang et al., 2004). The increasing boundary layer depth resulting from the urban heat island effect facilitates the cloud condensation at the top of the mixing layer over the convection initiation location (Li et al., 2017b; Yang et al., 2013). The aerosol loading from the urban area affects the microphysical processes of the thunderclouds as well as the occurrence of lightning (Sun et al., 2020a). The synergy of thermodynamic and microphysical processes may substantially modify the thunderstorm evolution in the urban area when thunderstorms spread from the northwest mountainous area to the urban area, increase the effectiveness of charge separation and electrification processes, and enhance lightning activity over the urban area, accordingly. It is worthy of further in-depth research, how and how much the convection is enhanced when the thunderstorm passes through the urban area of Beijing.

5. Lightning data application in severe weather nowcasting and assimilation in numerical models

Lightning largely depends on the thermodynamic and microphysical processes in thunderclouds. Therefore, as mentioned above, severe thunderstorms not only produce a high ratio of lightning but also often produce severe weather, such as hailfall, damaging winds, short-duration heavy rainfall, and so on. At the same time, the severe thunderstorms that generate these disastrous and severe weather events are usually accompanied by high lighting frequency and unique lightning characteristics. This indicates the potential importance of the application of lightning activity in the nowcasting of severe weather.

Lightning can be a predictor for hailfall nowcasting. For the 20160610 multicell hailstorm (see Figure 4), the total lightning and IC flash ratio of the whole process was high, and the ratio of +CG flashes to total CG flashes was much greater than that of usual thunderstorms. Before the second to fifth hailfall stages, the ratio of +CG flashes increased substantially, especially during the fifth hailfall stage, when the proportion of +CG flashes exceeded 50%. The flash ratio before the second, third, and fifth hailfall stages all increased significantly, all past the 2σ lightning jump criteria (Schultz et al., 2009; Sun et al., 2020b). On the basis of the total lightning activity from the BLNET, a total of 148 hailfall events were tested as a nowcasting experiment. It was found that most of the hailstorms produced a high flash rate, a significant increase in flash rate can be observed before the hailfall event, and there was a lightning jump preceding 81.8% of all hailfall events with an average lead time of 27.1 min (Tian et al., 2019). Therefore, the 2σ lightning jump algorithm is a good predictor for hail nowcasting.

Lightning and convective precipitation usually accompany each other. In some thunderstorm systems, there is good correlation between the two (Wu et al., 2017; Li et al., 2017a). A nowcasting method of short-duration heavy rainfall (i.e., <6 h) events was proposed based on a relationship between rainfall and lightning jumps (Wu et al., 2018). The proposed approach can provide early warning of short-duration heavy rainfall events from the meso-γ-scale to the regional scale, indicating the potential application in regions

where high-resolution total lightning observations are available.

The lightning location data have been examined as a new data assimilation source in cloud-resolving numerical models to improve the forecasting of severe convection and precipitation. Several studies have demonstrated the benefit of lightning data assimilation. The relationships between lightning data and other meteorological variables, such as water vapor, graupel mass, updraft volume, and proxy radar reflectivity have been examined. A new lightning data assimilation scheme with comprehensive nudging water content was developed, including water vapor in the low level of 900–700 hPa and graupel mass in the mixing phase region (Chen et al., 2019). The nudging functions for the water vapor mixing ratio (Q_v, g kg^{-1}) and graupel mixing ratio (Q_g, g kg^{-1}) are as follows:

$$\begin{aligned} Q_v &= aQ_{sat} + 0.2Q_{sat}\tanh(0.05X)\left[1-\tanh(cQ^{\alpha}_{g\_model})\right], \\ Q_g &= b + 0.002\tanh(0.05X)\left[1-\tanh(cQ^{\alpha}_{g\_model})\right], \end{aligned} \quad (1)$$

where Q_{sat} and Q_{g_model} represent the saturation mixing ratio of water vapor and graupel of the model predictions, respectively, X is the flash rate, and a, b, c, and α are constants. The simulation-based on the WRF (Weather Research and Forecasting) model showed that extra moisture was added in the lower altitudes, and the convection developed toward the higher layers and sustained its development over a longer period after the lightning data assimilation, resulting in a significant improvement in the quantitative precipitation forecasts.

The 3DVAR (3 Dimensional Variational Assimilation) lightning assimilation method is also examined in the WRF-3DVAR model in a cycling mode with an interval of 10 min based on empirical functions between the lightning rate and mixing ratio of water vapor (Zhang R et al., 2017). It is suggested that the forecasting of the 3 h accumulative precipitation can be greatly improved via the 3DVAR technique, and 60 min is an appropriate time window for lightning assimilation for a squall line system. Lightning-proxy relative humidity with WRF-3DVAR also shows some improvements in the forecasting of both reflectivity and precipitation, and temperature, dew-point temperature, and relative humidity profiles are also improved after 7 h (Wang et al., 2017). Xiao et al. (2018) established the empirical relationship between the total flash ratio and the maximum value of vertical velocity and introduced it into the VDRAS (Variational Doppler Radar Analysis System) model utilizing 4DVAR. The assimilation of lightning data increases the vertical velocity of the middle layer and thus brings strong vertical movement and latent heat release to the entire inversion area, thereby helping to maintain the development of convective storms and promote the generation of new convection. This study also suggested that lightning data assimilation is conducive to suppress false precipitation predictions to some extent.

The radar reflectivity observation operator has been developed for many data assimilation systems, so lightning-proxy radar reflectivity can improve the simulation of existing schemes in the model without having to develop a new observation operator. Due to the accumulation of ground flash location data in China for many years, and the large spatial coverage, the proxy radar reflectivity based on the ground flash frequency can also achieve lightning data assimilation through physical initialization methods (Wang et al., 2014; Yang et al., 2015), thereby improving the accuracy of convective forecasting.

Lightning activity is substantially affected by thermodynamic and microphysical processes (Liu et al., 2014; Wang et al., 2015a, 2015b; Xu L T et al., 2016; Zhao et al., 2015), hence lightning can be predicted based on thermodynamic and microphysical parameters. A modified lightning potential index (MLPI) has been proposed and used to forecast the genesis of lightning (Li et al., 2016). The lightning density is estimated using the ice masses of precipitation and non-precipitation. Simulations with the WRF model for quasi-linear MCSs show that lightning flashes are likely to occur in the regions with a large CAPE gradient, and that most lightning flashes are produced on the right side and at the front of the MCSs, where the surface wind field converges intensely.

6. Conclusion and future studies

With the aim of mitigating meteorological hazards in China, the STORM973 project conducted a five-year campaign to study a variety of thunderstorm types in the Beijing region, using the BLNET 3D lightning location system and the polarimetric and Doppler radar observations. The lightning location data from the BLNET has the advantages of 3D location of both IC and CG lightning with high-precision and being free from the terrain influences, providing new insights into the structure of the severe thunderstorms, especially the cluster meso-γ-scale cell storms.

Observational studies have found that squall line systems with long duration and large impact range are the strongest type of severe thunderstorm affecting Beijing. Owing to the large area of the convection line in the front, heavy precipitation could be disastrous for a large area. The lightning frequency can be as high as hundreds of flashes per minute. The observations also found that multicell thunderstorms with multiple meso-γ-scale cells are also an important type of severe thunderstorm affecting Beijing. The outburst of meso-γ-scale cells is rapid and their accurate prediction is difficult. Multiple meso-γ-scale individual cells occur simultaneously or successively in different locations, increasing the diffi-

culty of forecasting and heavily impacting human activities in Beijing. Furthermore, although supercell thunderstorms do not occur frequently in the BMR, owing to their intensive convection, large range, and high lightning frequency, the impact is profound when they do occur. The comprehensive observations, including the BLNET 3D lightning radiation source location, X-band dual-linear polarization Doppler radar, and other detection methods, have great advantages for the observation of meso-γ-scale convective cells with small time and space resolution. It is helpful to deeply understand the development and evolution of small-scale severe thunderstorms, and lightning observations can also compensate for the deficiencies of radar ground blockage, short-range blind spots, and heavy precipitation attenuation to some extent.

In addition, preliminary research results have found that lightning location data can be used as a new data assimilation source for numerical prediction models, which is of great significance for improving the prediction effect of strong convection and heavy precipitation. Besides, the rapid increase in lightning frequency has some nowcasting indication for ground hail and short-term heavy precipitation events. At present, appearance of a hailstorm mainly relies on particle classification recognition of polarized radar, and hail records are mainly recorded manually at weather stations, which is one of the few meteorological elements that still retains manual records. Lightning data can be a good supplementary for hailstorm identification and nowcasting, and it is worth further research.

Certainly, the key to determining the interrelationships among lightning, kinematics, and microphysics in thunderstorms is to identify and understand the charge structure inside the thundercloud. However, it is not feasible to fly sounding balloons in the BMR because of public safety requirements. The 3D location on the lightning radiation sources can identify the charge region in the cloud and is expected to play an important role in future research. Owing to the attenuation by heavy precipitation for the X-band dual-polarization radar detection, the 20150727 and 20170811 processes could not be analyzed with identifying the hydrometeor particles. Recently, based on the 3D lightning location and X-band dual linear polarization Doppler radar data, Liu et al. (2020) discussed the relationship between lightning and ice particles in the mixed-phase region for the 20170613 supercell thunderstorm. It is crucial to reveal the common kinematic, microphysical, and lightning characteristics of diverse kinds of thunderstorms. The relationship between lightning and strong updraft, ice particles, water vapor content in the lower and middle troposphere, vertical wind shear, and so on will be further studied for more cases in the future. In addition, it is necessary to understand the combined effects of topography and urbanization on severe thunderstorm intensification in the BMR. The joint influence of the urban heat island effect, complex underlying surface, and aerosol loading on the initiation and evolution of thunderstorms is a primary research task that is also still ongoing.

Acknowledgements *The authors thank all those who participated in the observation, data collection and processing of "STORM973". This work was supported by the National Natural Science Foundation of China (Grant Nos. 41630425, 41671144074), the Key Research Program of Frontier Science, CAS (Grant No. QYZDJ-SSW-DQC007) and the National Key Basic Research Program of China (Grant No. 2014CB441401).*

References

Chan Y T, Ho K C. 1994. A simple and efficient estimator for hyperbolic location. IEEE Trans Signal Process, 42: 1905–1915

Chen S, Zhang Y, Chen C, Yan X, Lu W, Zhang Y. 2016. Influence of the ground potential rise on the residual voltage of low-voltage surge protective devices due to nearby lightning flashes. IEEE Trans Power Deliver, 31: 596–604

Chen S, Zhang Y, Zhou M, Yan X, Lu W, Chen L, Zhang Y. 2018a. Observation of residual voltage in low-voltage surge protective devices due to nearby M-components. IEEE Trans Electromagn Compat, 60: 776–784

Chen S, Zhang Y, Zhou M, Yan X, Lu W, Zhang Y. 2018b. Influence on low-voltage surge protective devices of overhead distribution lines due to nearby return strokes. IEEE Trans Power Deliver, 33: 1099–1106

Chen Z, Qie X, Liu D, Xiong Y. 2019. Lightning data assimilation with comprehensively nudging water contents at cloud-resolving scale using WRF model. Atmos Res, 221: 72–87

Chen Z, Qie X, Yair Y, Liu D, Xiao X, Wang D, Yuan Y. 2020. Electrical evolution of a rapidly developing MCS during its vigorous vertical growth phase. Atmos Res, 246: 105201, doi: 10.1016/j.atmosres.2020.105201

Fan Y, Lu G, Li X, Zheng T, Zhang H, Jiang R, Liu M, Qie X, Zhang Y, Zhang Y, Lyu W, Zheng D. 2019. Measurements of burst of magnetic pulses during the initial continuous current in rocket-triggered lightning. J Geophys Res-Atmos, 124: 11710–11721

Fan Y, Lu G, Jiang R, Zhang H, Li X, Liu M, Qie X, Zheng D, Lyu W, Zhang Y, Zhang Y. 2018. Characteristics of electromagnetic signals during the initial stage of rocket-triggered lightning. J Geophys Res-Atmos, 123: 11625–11636

Feng G, Qie X, Yuan T, Niu S. 2007. Lightning activity and precipitation structure of hailstorms. Sci China Ser D-Earth Sci, 50: 629–639

Feng L, Xiao H, Sun Y. 2018. A study on hydrometeor classification and application based on X-band dual-polarization radar measurements (in Chinese). Clim Environ Res, 23: 366–386

Gao Y, Lu W, Ma Y, Chen L, Zhang Y, Yan X, Zhang Y. 2014. Three-dimensional propagation characteristics of the upward connecting leaders in six negative tall-object flashes in Guangzhou. Atmos Res, 149: 193–203

Guo F X, Li Y, Huang Z C, Wang M F, Zeng F H, Lian C H, Mu Y J. 2017. Numerical simulation of 23 June 2016 Yancheng City EF4 tornadic supercell and analysis of lightning activity. Sci China Earth Sci, 60: 2204–2213

Jiang R, Qie X, Wu Z, Wang D, Liu M, Lu G, Liu D. 2014. Characteristics of upward lightning from a 325-m-tall meteorology tower. Atmos Res, 149: 111–119

Jiang R, Qie X, Zhang H, Liu M, Sun Z, Lu G, Wang Z, Wang Y. 2017. Channel branching and zigzagging in negative cloud-to-ground lightning. Sci Rep, 7: 3457

Lang T J, Miller L J, Weisman M, Rutledge S A, Barker Llyle J. I, Bringi V N, Chandrasekar V, Detwiler A, Doesken N, Helsdon J, Knight C, Krehbiel P, Lyons W A, Macgorman D, Rasmussen E, Rison W, Rust W D, Thomas R J. 2004. The severe thunderstorm electrification and precipitation study. Bull Amer Meteorol Soc, 85: 1107–1126

Li H, Cui X, Zhang D L. 2017a. A statistical analysis of hourly heavy rainfall events over the Beijing metropolitan region during the warm seasons of 2007–2014. Int J Climatol, 37: 4027–4042
Li H, Cui X, Zhang D L. 2017b. Sensitivity of the initiation of an isolated thunderstorm over the Beijing metropolitan region to urbanization, terrain morphology and cold outflows. Q J R Meteorol Soc, 143: 3153–3164
Li W, Qie X, Fu S, Su D, Shen Y. 2016. Simulation of quasi-linear mesoscale convective systems in northern China: Lightning activities and storm structure. Adv Atmos Sci, 33: 85–100
Li X, Zhang Q, Zou T, Lin J, Kong H, Ren Z. 2018. Climatology of hail frequency and size in China, 1980–2015. J Appl Meteorol Climatol, 57: 875–887
Li Y, Zhang G, Wang Y, Wu B, Li J. 2017. Observation and analysis of electrical structure change and diversity in thunderstorms on the Qinghai-Tibet Plateau. Atmos Res, 194: 130–141
Liang X, Miao S, Li J, Bornstein R, Zhang X, Gao Y, Chen F, Cao X, Cheng Z, Clements C, Dabberdt W, Ding A, Ding D, Dou J J, Dou J X, Dou Y, Grimmond C S B, González-Cruz J E, He J, Huang M, Huang X, Ju S, Li Q, Niyogi D, Quan J, Sun J, Sun J Z, Yu M, Zhang J, Zhang Y, Zhao X, Zheng Z, Zhou M. 2018. SURF: Understanding and predicting urban convection and haze. Bull Am Meteorol Soc, 99: 1391–1413
Liu D, Qie X, Chen Y, Sun Z, Yuan S. 2020. Investigating lightning characteristics through a supercell storm by comprehensive coordinated observations over north China. Adv Atmos Sci, doi: 10.1007/s00376-020-9264-x
Liu D, Qie X, Peng L, Li W. 2014. Charge structure of a summer thunderstorm in North China: Simulation using a Regional Atmospheric Model System. Adv Atmos Sci, 31: 1022–1034
Logan T. 2018. Anomalous lightning behavior during the 26–27 August 2007 Northern Great Plains severe weather event. J Geophys Res-Atmos, 123: 1771–1784
Lu G, Fan Y, Zhang H, Jiang R, Liu M, Qie X, Cummer S A, Han C, Liu K. 2018. Measurement of continuing charge transfer in rocket-triggered lightning with low-frequency magnetic sensor at close range. J Atmos Sol-Terrestrial Phys, 175: 76–86
Lu G, Zhang H, Jiang R, Fan Y, Qie X, Liu M, Sun Z, Wang Z, Tian Y, Liu K. 2016. Characterization of initial current pulses in negative rocket-triggered lightning with sensitive magnetic sensor. Radio Sci, 51: 1432–1444
Lu W, Gao Y, Chen L, Qi Q, Ma Y, Zhang Y, Chen S, Yan X, Chen C, Zhang Y. 2015. Three-dimensional propagation characteristics of the leaders in the attachment process of a downward negative lightning flash. J Atmos Sol-Terrestrial Phys, 136: 23–30
Luo Y, Zhang R, Wan Q, Wang B, Wong W K, Hu Z, Jou B J D, Lin Y, Johnson R H, Chang C P, Zhu Y, Zhang X, Wang H, Xia R, Ma J, Zhang D L, Gao M, Zhang Y, Liu X, Chen Y, Huang H, Bao X, Ruan Z, Cui Z, Meng Z, Sun J, Wu M, Wang H, Peng X, Qian W, Zhao K, Xiao Y. 2017. The Southern China Monsoon Rainfall Experiment (SCMREX). Bull Am Meteorol Soc, 98: 999–1013
Ma M, Lu W, Zhang Y, Meng Q. 2008. Analysis of lightning disaster in China and their correlative factors (in Chinese). Adv Earth Sci, 23: 856–865
Meng Z, Zhang F, Luo D, Tan Z, Fang J, Sun J, Shen X, Zhang Y, Wang S, Han W, Zhao K, Zhu L, Hu Y, Xue H, Ma Y, Zhang L, Nie J, Zhou R, Li S, Liu H, Zhu Y. 2019. Review of Chinese atmospheric science research over the past 70 years: Synoptic meteorology. Sci China Earth Sci, 62: 1946–1991
Miao S, Chen F, Li Q, Fan S. 2011. Impacts of urban processes and urbanization on summer precipitation: A case study of heavy rainfall in Beijing on 1 August 2006. J Appl Meteorol Climatol, 50: 806–825
Mu M, Duan W S, Tang Y M. 2017. The predictability of atmospheric and oceanic motions: Retrospect and prospects. Sci China Earth Sci, 60: 2001–2012
Pu Y, Jiang R, Qie X, Liu M, Zhang H, Fan Y, Wu X. 2017. Upward negative leaders in positive triggered lightning: Stepping and branching in the initial stage. Geophys Res Lett, 44: 7029–7035
Pu Y, Qie X, Jiang R, Sun Z, Liu M, Zhang H. 2019. Broadband characteristics of chaotic pulse trains associated with sequential dart leaders in a rocket-triggered lightning flash. J Geophys Res-Atmos, 124: 4074–4085
Qi Q, Lu W, Ma Y, Chen L, Zhang Y, Rakov V A. 2016. High-speed video observations of the fine structure of a natural negative stepped leader at close distance. Atmos Res, 178–179: 260–267
Qie X, Pu Y, Jiang R, Sun Z, Liu M, Zhang H, Li X, Lu G, Tian Y. 2017. Bidirectional leader development in a preexisting channel as observed in rocket-triggered lightning flashes. J Geophys Res-Atmos, 122: 586–599
Qie X, Zhang Y. 2019. A review of atmospheric electricity research in China from 2011 to 2018. Adv Atmos Sci, 36: 994–1014
Ribaud J F, Bousquet O, Coquillat S. 2016. Relationships between total lightning activity, microphysics and kinematics during the 24 September 2012 HyMeX bow-echo system. Q J R Meteorol Soc, 142: 298–309
Saunders C P R, Peck S L. 1998. Laboratory studies of the influence of the rime accretion rate on charge transfer during crystal/graupel collisions. J Geophys Res, 103: 13949–13956
Schultz C J, Petersen W A, Carey L D. 2009. Preliminary development and evaluation of lightning jump algorithms for the real-time detection of severe weather. J Appl Meteorol Climatol, 48: 2543–2563
Shepherd J M. 2005. A review of current investigations of urban- induced rainfall and recommendations for the future. Earth Interact, 9: 1–27
Srivastava A, Tian Y, Qie X, Wang D, Sun Z, Yuan S, Wang Y, Chen Z, Xu W, Zhang H, Jiang R, Su D. 2017. Performance assessment of Beijing Lightning Network (BLNET) and comparison with other lightning location networks across Beijing. Atmos Res, 197: 76–83
Sun J, Chen M, Wang Y. 2010. A frequent-updating analysis system based on radar, surface, and mesoscale model data for the Beijing 2008 Forecast Demonstration Project. Weather Forecast, 25: 1715–1735
Sun J, Lei L, Yu B, Ding Q. 2015. The fundamental features of the extreme severe rain events in the recent 10 years in the Beijing area (in Chinese). Acta Meteorol Sin,73: 609–623
Sun L, Chen Z, Xu Y, Sun Z, Yuan S, Wang D, Tian Y, Xu W, Qie X. 2019. Evolution of lightning radiation sources of a strong quall line over Beijing metropolitan region and its relation to convection region and surface thermodynamic condition (in Chinese). Chin J Atmos Sci, 43: 759–772
Sun L, Qie X, Mansell E, Chen Z, Xu Y, Jiang R, Sun Z. 2018. Feedback effect of electric force on electrification and charge structure in thunderstorm (in Chinese). Acta Phys Sin, 67: 371–383
Sun M, Qie X, Liu D, Yoav Y, Xia X, Yuan S, Wang D, Lu J, Srivastava1 A, Ntwali D. 2020a. Analysis of potential effects of aerosol on lightning activity in Beijing metropolitan region (in Chinese). Chin J Geophys, 63: 1766–1774
Sun M, Qie X, Sun L, Liu D, Wang D, Yuan S, Chen Z, Xu W, Sun C, Su D. 2020b. Lightning activity of a severe thunderstorm with several hailfall stages in Beijing Metropolitan Region (in Chinese). Chin J Atmos Sci, 44: 601–610
Sun Z, Qie X, Jiang R, Liu M, Wu X, Wang Z, Lu G, Zhang H. 2014. Characteristics of a rocket-triggered lightning flash with large stroke number and the associated leader propagation. J Geophys Res-Atmos, 119: 13388
Tian Y, Qie X, Sun Y, Wang D, Yuan S, Sun Z, Lu G, Yu L, Sun H, Li L, Du C. 2019. Total lightning signatures of thunderstorms and lightning jumps in hailfall nowcasting in the Beijing area. Atmos Res, 230: 104646
Wang D, Qie X, Yuan S, Sun Z, Chen Z, Li J, Zhang H, Liu M, Srivastava A, Liu D. 2020. Spatial and temporal distribution of lightning activity and contribution of thunderstorms with different lightning-producing capabilities in Beijing Metropolitan Region (in Chinese). Chin J Atmos Sci, 44: 225–238
Wang F, Zhang Y, Zheng D, Xu L. 2015a. Impact of the vertical velocity field on charging processes and charge separation in a simulated thunderstorm. J Meteorol Res, 29: 328–343

Wang F, Zhang Y, Zheng D. 2015b. Impact of updraft on neutralized charge rate by lightning in thunderstorms: A simulation case study. J Meteorol Res, 29: 997–1010
Wang Y, Qie X, Wang D, Liu M, Su D, Wang Z, Liu D, Wu Z, Sun Z, Tian Y. 2016. Beijing Lightning Network (BLNET) and the observation on preliminary breakdown processes. Atmos Res, 171: 121–132
Wang Y, Yang Y, Liu D, Zhang D, Yao W, Wang C. 2017. A case study of assimilating lightning-proxy relative humidity with WRF-3DVAR. Atmosphere, 8: 55
Wang Y, Yang Y, Wang C. 2014. Improving forecasting of strong convection by assimilating cloud-to-ground lightning data using the physical initialization method. Atmos Res, 150: 31–41
Wang Z, Qie X, Jiang R, Wang C, Lu G, Sun Z, Liu M, Pu Y. 2016. High-speed video observation of stepwise propagation of a natural upward positive leader. J Geophys Res-Atmos, 121: 14307–14315
Wilson J W, Feng Y, Chen M, Roberts R D. 2010. Nowcasting challenges during the Beijing Olympics: Successes, failures, and implications for future nowcasting systems. Weather Forecast, 25: 1691–1714
Wu B, Zhang G, Wen J, Zhang T, Li Y, Wang Y. 2016. Correlation analysis between initial preliminary breakdown process, the characteristic of radiation pulse, and the charge structure on the Qinghai-Tibetan Plateau. J Geophys Res-Atmos, 121: 12434
Wu F, Cui X, Zhang D L. 2018. A lightning-based nowcast-warning approach for short-duration rainfall events: Development and testing over Beijing during the warm seasons of 2006–2007. Atmos Res, 205: 2–17
Wu F, Cui X, Zhang D L, Qiao L. 2017. The relationship of lightning activity and short-duration rainfall events during warm seasons over the Beijing metropolitan region. Atmos Res, 195: 31–43
Wu X K, Qie X S, Yuan T. 2013. Regional distribution and diurnal variation of deep convective systems over the Asian monsoon region. Sci China Earth Sci, 56: 843–854
Xia R, Zhang D L, Wang B. 2015. A 6-yr cloud-to-ground lightning climatology and its relationship to rainfall over central and eastern China. J Appl Meteorol Climatol, 54: 2443–2460
Xiao X, Sun J, Chen M, Qie X, Wang Y, Ying Z. 2017. The characteristics of weakly forced mountain-to-plain precipitation systems based on radar observations and high-resolution reanalysis. J Geophys Res-Atmos, 122: 3193–3213
Xiao X, Sun J, Chen M, Qie X, Ying Z, Wang Y, Ji L. 2019. Comparison of environmental and mesoscale characteristics of two types of mountain-to-plain precipitation systems in the Beijing region, China. J Geophys Res-Atmos, 124: 6856–6872
Xiao X, Sun J, Qie X, Ying Z, He J. 2018. A new lightning assimilation technique based on 4DVAR. San Francisco: AGU Fall Meeting
Xu L T, Zhang Y J, Liu H Y, Zheng D, Wang F. 2016. The role of dynamic transport in the formation of the inverted charge structure in a simulated hailstorm. Sci China Earth Sci, 59: 1414–1426
Xu S, Zheng D, Wang Y, Hu P. 2016. Characteristics of the two active stages of lightning activity in two hailstorms. J Meteorol Res, 30: 265–281
Xu Y, Sun Z, Zhou Y, Yuan S, Chen Z, Liu D, Wang D, Tian Y, Xu W, Qie X. 2018. Lightning activity of a severe squall line with cell merging process and its relationships with dynamic fields (in Chinese). Chin J Atmos Sci, 42: 1393–1406
Yang L, Tian F, Smith J A, Hu H. 2014. Urban signatures in the spatial clustering of summer heavy rainfall events over the Beijing metropolitan region. J Geophys Res-Atmos, 119: 1203–1217
Yang P, Ren G, Hou W, Liu W. 2013. Spatial and diurnal characteristics of summer rainfall over Beijing Municipality based on a high-density AWS dataset. Int J Climatol, 33: 2769–2780
Yang X, Sun J. 2018. Organizational modes of severe wind-producing convective systems over North China. Adv Atmos Sci, 35: 540–549
Yang Y, Wang Y, Zhu K. 2015. Assimilation of Chinese doppler radar and lightning data using WRF-GSI: A case study of mesoscale convective system. Adv Meteorol, 2015: 1–17
Yu M, Miao S, Li Q. 2017. Synoptic analysis and urban signatures of a heavy rainfall on 7 August 2015 in Beijing. J Geophys Res-Atmos, 122: 65–78
Yuan S, Jiang R, Qie X, Wang D, Sun Z, Liu M. 2017. Characteristics of upward lightning on the Beijing 325 m meteorology tower and corresponding thunderstorm conditions. J Geophys Res-Atmos, 122: 12093
Yuan S, Qie X, Jiang R, Wang D, Sun Z, Srivastava A, Williams E. 2020. Origin of an uncommon multiple-stroke positive cloud-to-ground lightning flash with different terminations. J Geophys Res-Atmos, 125: e2019JD032098, doi: 10.1029/2019JD032098
Zhang C, Lu W, Chen L, Qi Q, Ma Y, Yao W, Zhang Y. 2017. Influence of the Canton Tower on the cloud-to-ground lightning in its vicinity. J Geophys Res-Atmos, 122: 5943–5954
Zhang D L. 2020. Rapid urbanization and more extreme rainfall events. Sci Bull, 65: 516–518
Zhang R, Ni Y, Liu L, Luo Y, Wang Y. 2011. South China Heavy Rainfall Experiments (SCHeREX). J Meteorol Soc Jpn, 89A: 153–166
Zhang R, Zhang Y, Xu L, Zheng D, Yao W. 2017. Assimilation of total lightning data using the three-dimensional variational method at convection-allowing resolution. J Meteorol Res, 31: 731–746
Zhang Y, Krehbiel P R, Zhang Y, Lu W, Zheng D, Xu L, Huang Z. 2017. Observations of the initial stage of a rocket-and-wire-triggered lightning discharge. Geophys Res Lett, 44: 4332–4340
Zhang Y, Zhang Y J, Zheng D, Lu W. 2018. Characteristics and discharge processes of M events with large current in triggered lightning. Radio Sci, 53: 974–985
Zhao P, Yin Y, Xiao H. 2015. The effects of aerosol on development of thunderstorm electrification: A numerical study. Atmos Res, 153: 376–391

(Responsible editor: Hongsheng ZHANG)